Supplementary Information: Synthesis and structure of temperature-sensitive nanocapsules

Monia Brugnoni,[1] Fabian Fink,[1] Andrea Scotti,[1] and Walter Richtering[1]
[1] *Institute of Physical Chemistry, RWTH Aachen University, 52056 Aachen, Germany*

1. EXPERIMENTAL SECTION

1.1. Synthesis of P(NIPAM-co-NtBAM) Microgels

P(NIPAM-co-NtBAM) microgels were prepared from precipitation polymerization of NIPAM, NtBAM and BIS. Two different molar NIPAM:NtBAM:BIS ratios were chosen: 0.65:0.30:0.05 (referred to as 30%NtBAM) and 0.57:0.38:0.05 (referred to as 38%NtBAM). The monomers and SDS were dissolved according to table S.1 in water. The solution was purged with nitrogen and preheated to 60 °C under constant stirring. The initiator solution of 63.4 mg of KPS in 5 mL of water was degassed simultaneously. It was introduced at once into the monomer solution to initiate the reactions. The polymerizations were let to proceed for 2 hours at 60 °C and constant stirring. After cooling to room temperature, the microgels were purified by threefold centrifugation at 30 000 rpm and redispersion in fresh water. Lyophilization was applied for storage.

Silica-core p(NIPAM-co-NtBAM)-shell microgels were prepared similarly to the pure p(NIPAM-co-NtBAM) microgels in presence of 1.9256 g (0.3472 g) of the silica nanoparticles redispersed in 5 mL of ethanol during the polymerization of the 5 (10) mol% cross-linked core-shell (CS-5 and CS-10) and the reactions were started by addition of 126.1 mg (22.8 mg) of KPS dissolved in 5 mL of water.
The corresponding hollow microgels were obtained from NaOH treatment of the core-shell microgels, which results in a complete core dissolution. [1, 2] Purification by dialysis resulted in aggregation of the samples.

TABLE S.1. Composition of reaction solutions during synthesis of regular p(NIPAM-co-NtBAM) and silica-core p(NIPAM-co-NtBAM)-shell microgels.

Microgel	m**(NIPAM)** **(g)**	m**(NtBAM)** **(g)**	m**(BIS)** **(g)**	m**(SDS)** **(mg)**	$V_{\mathbf{total}}$ **(mL)**
30%NtBAM	4.6452	2.4095	0.4868	65.4	150
38%NtBAM	4.0732	3.0518	0.4868	34.6	175
CS-5	0.9372	0.7021	0.1121	–	305
CS-10	0.1600	0.1200	0.0405	–	55

1.2. ^{1}H NMR Spectroscopy

^{1}H nuclear magnetic resonance (^{1}H NMR) spectroscopy was performed on a 400 MHz Bruker DRX NMR spectrometer. All samples were probed in D_2O at room temperature.

2. P(NIPAM-CO-NTBAM) MICROGELS

2.1. Regular Microgels

NtBAM is more hydrophobic than NIPAM due to the non-polar *tert*-butyl group (see figure S.1). The co-polymerization of NIPAM and NtBAM leads to co-polymeric microgels whose VPTTs are shifted toward lower temperatures when compared to the VPTT of homopolymeric pNIPAM microgels. [3] Therefore, first, syntheses of regular microgels are performed to determine a reasonable monomer composition in order to lower the VPTT.

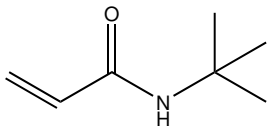

FIG. S.1. Chemical structure of the *N-tert*-butylacrylamide (NtBAM) monomer.

Two distinct monomer compositions were chosen, namely molar NIPAM:NtBAM:BIS ratios of 0.57:0.38:0.05 (referred to as 38%NtBAM) and 0.65:0.30:0.05 (referred to as 30%NtBAM). The higher the NtBAM amount, the more hydrophobic is the polymer network and the lower is the VPTT. It is important to note that the water solubility of NtBAM is rather restricted even at high temperature, which affects the reproducibility of the syntheses.

Figure S.2 shows the hydrodynamic radius, R_h, as a function of the temperature, T, of the two microgel samples: 38%NtBAM (*squares*) and 30%NtBAM (*circles*). The curves reveal the typical temperature-dependent size changes known from thermoresponsive microgels.

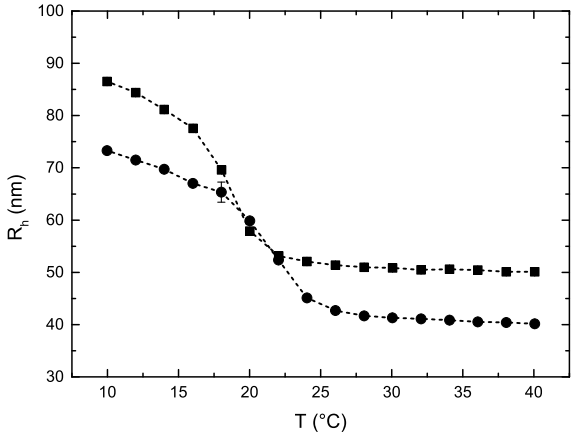

FIG. S.2. Hydrodynamic radius, R_h, as a function of the temperature, T, of 30%NtBAM (*circles*) and 38%NtBAM (*squares*) microgels.

Compared to pure pNIPAM microgels, both co-polymeric microgels possess a considerable lower VPTT of 20 °C for the 30%NtBAM microgels and 17 °C for the 38%NtBAM. SDS was added during the polymerization reactions to ensure stable polymer globule formation. Therefore, the total radii of the microgels are rather small. When assuming that the microgels are fully swollen at 10 °C, swelling ratios of $Q(30\%\mathrm{NtBAM}) = 1.78 \pm 0.01$ and $Q(38\%\mathrm{NtBAM}) = 1.72 \pm 0.01$ are obtained.
In the following, the composition of the 38%NtBAM microgels is chosen to produce hollow microgels ensuring the deswollen swelling state at room temperature. The VPTT allows to obtain the swollen state of the microgels by cooling the microgel solutions *e.g.* in a refrigerator.

2.2. Hollow Microgels

Hollow p(NIPAM-co-NtBAM) microgels were synthesized as described in the Experimental Section. A p(NIPAM-co-NtBAM) shell is added onto surface modified silica nanoparticles with a radius of about 60 nm, which can be dissolved by NaOH etching to obtain hollow nanocapsules. Microgels were produced with 5 mol% and 10 mol% cross-linking density and identical NIPAM:NtBAM ratio.
Figure S.3 shows the results obtained from dynamic light scattering. Figure S.3A illustrates the hydrodynamic radius as a function of temperature of the 5 mol% cross-linked core-shell (*full circles*) and the corresponding hollow (*open circles*) microgels. As expected, the VPTTs of both microgels are below room temperature. However, the core-shell microgels are considerably smaller than the hollow microgels and reveal a much lower swelling ability. This trend is already known for hollow microgels but not to this extent. [4] A possible reason is a loss of integrity of the polymeric shell. In contrast, the 10 mol% cross-linked core-shell (*full triangles*) and corresponding unpurified hollow (*open triangles*) microgels shown in figure S.3B do not show this considerable difference of the swelling behaviors. The hollow microgels still swell more than the core-shell counterpart, but collapse to a comparable size. This is commonly observed for highly cross-linked hollow microgels. [2]

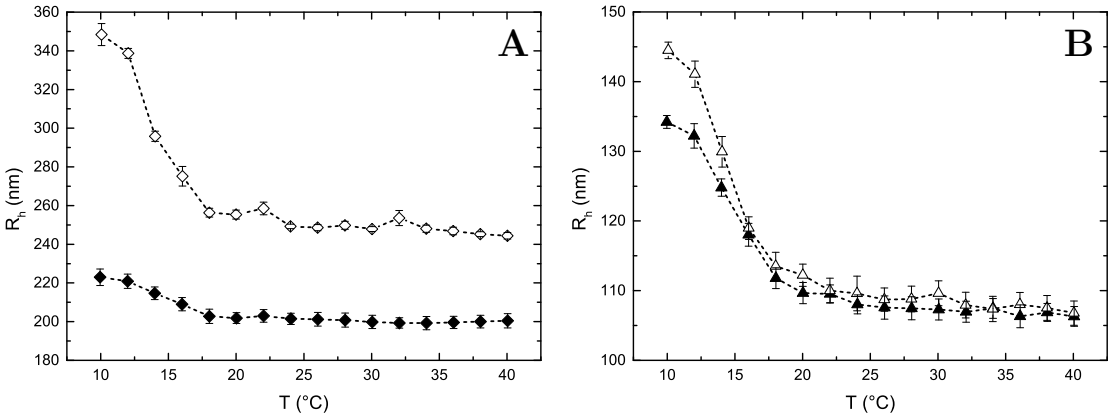

FIG. S.3. Hydrodynamic radius, R_h, as a function of the temperature, T, of silica-core p(NIPAM-co-NtBAM)-shell (*full symbols*) and the corresponding hollow (*open symbols*) microgels with **(A)** 5 mol% and **(B)** 10 mol% cross-linking density.

At high dilutions (as used in DLS), the microgels solutions are stable even above the VPTT. However, figure S.4 shows the various p(NIPAM-co-NtBAM) microgels in water at room temperature. It reveals that all microgel solutions, except the regular 30%NtBAM microgels, form large aggregates after a certain amount of time indicating that the microgels are not colloidally stable. Structural analysis by *e.g.* static light scattering is precluded by the aggregation.

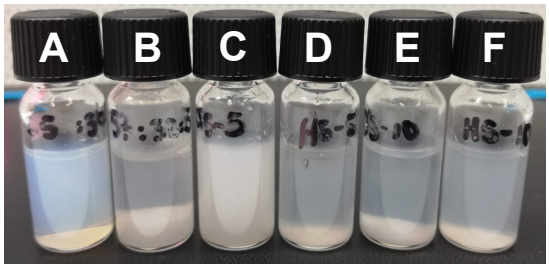

FIG. S.4. Solutions of **(A)** 30%NtBAM, **(B)** 38%NtBAM, **(C)** 5 mol% cross-linked core-shell and **(D)** corresponding hollow microgels, **(E)** 10 mol% cross-linked core-shell and **(F)** corresponding hollow microgels stored at room temperature. Only **(A)** shows a stable microgel solution. All other samples reveal aggregates at the bottom of the vials.

3. DAAM INCORPORATION IN ULTRA-LOW CROSS-LINKED MICROGELS

In the following, the results from the synthesis of p(NIPAM-co-DAAM) ULC (ULC-DAAM) microgels comprising 1 mol% DAAM are presented and compared to pure pNIPAM ULC microgels as presented in references [5], [6] and [7].

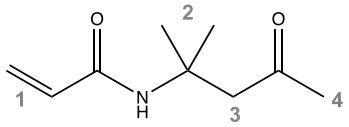

FIG. S.5. Chemical structure of the diacetone acrylamide (DAAM) monomer. The numbers serve for the assignment of ^{1}H NMR signals.

Figure S.6 shows the ^{1}H NMR spectra of the ULC-DAAM microgels (*green*) and for comparison of a pure pNIPAM ULC microgel (*black*) and the DAAM monomer (*orange*). The successful DAAM incorporation can be deduced when comparing the ULC-DAAM to the pNIPAM ULC microgels. There are three arising signals, which are also present in the spectrum of the DAAM monomer: the signals at a chemical shift of 1.30 ppm result from the six hydrogen atoms of the methyl groups in position 2 (see figure S.5 for the positions), at 2.18 ppm from the three hydrogen atoms in position 4 and at 3.04 ppm of the two hydrogens at position 3. The peaks above 5 ppm of the DAAM monomer correspond to the hydrogen atoms at the vinyl group (position 1), their signals shift toward lower values due to the polymerization reaction. The large signal at a chemical shift of 4.80 ppm result from the D_2O used as solvent.

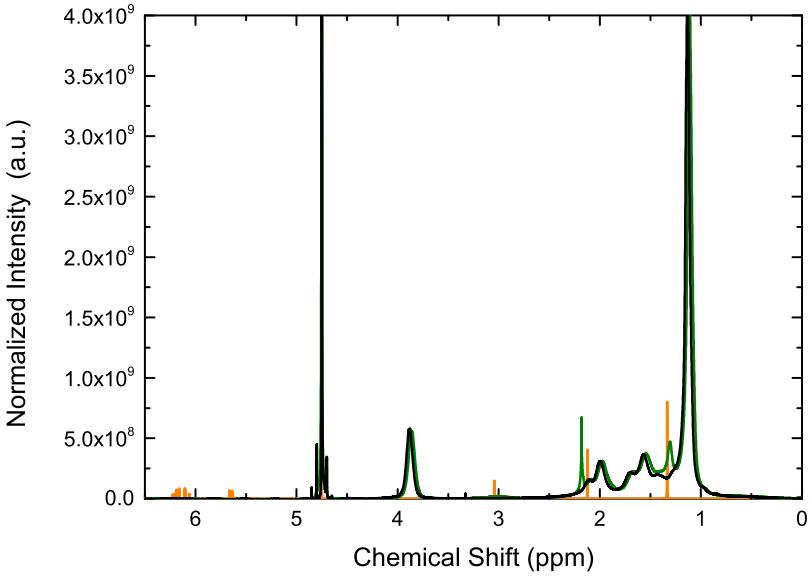

FIG. S.6. ^{1}H NMR spectrum of the pNIPAM ULC (*black*) and ULC-DAAM (*green*) microgels. The spectrum of the pure DAAM monomer (*orange*) is shown for reference.

4. SCATTERING INTENSITY OF HOLLOW MICROGELS WITH FITS OF THE FUZZY SPHERE MODEL

Figure S.7 illustrates the form factors of the hollow p(NIPAM-co-DAAM) microgels as already described in the main article. The *red lines*represent the fits with the form factor model by Stieger et al. describing a sphere with fuzzy periphery. [8] It can clearly be seen that the model is not appropriate to describe the experimental data. A hollow model is required as presented in the main article.

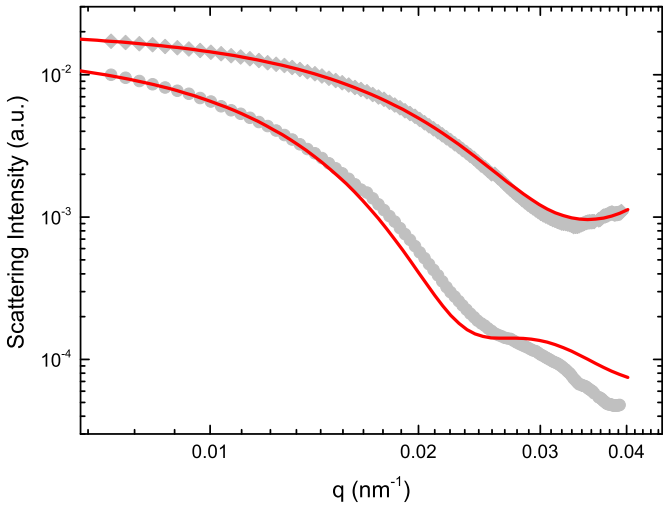

FIG. S.7. Scattering intensity as a function of the scattering vector, q, of the hollow p(NIPAM-co-DAAM) microgels probed at 30 °C (*diamonds*) and 10 °C (*circles*). The fits from the fuzzysphere model are represented by the *red lines* [8].

5. TRANSMISSION ELECTRON MICROSCOPY OF CORE-SHELL AND HOLLOW MICROGELS

Transmission electron microscopy (TEM) measurements were performed on a Carl Zeiss Libra 120 microscope operating at a voltage of 120 kV with a bottom mounted CCD camera. Zero-loss energy-filtered transmission electron microscopy was applied. 4 μL of the microgel dispersion was transferred onto a carbon coated TEM grid and left to dry. The samples were transferred into the microscope and let to equilibrate before starting the measurements.

Figure S.8 shows the micrographs obtained from TEM of both silica-core p(NIPAM-co-DAAM)-shell pNIPAM-shell (*left*) and corresponding hollow microgel (*right*). The images were recorded during the core dissolution process. This explains the shape of the silica-core, which can be identified as dark center surrounded by the polymeric shell of lower contrast. The cavity of the hollow microgels can be spotted as the light area in the center of the polymeric shell indicating a hollow microgel structure as targeted.
In TEM, the microgels are in their dried state absorbed onto a solid substrate, this leads to deformation. Thus, the structure cannot be compared to bulk experiments. Additionally the statistics in TEM are rather poor when compared to scattering experiments.

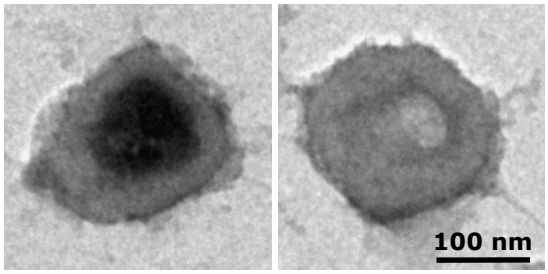

FIG. S.8. TEM micrographs of a silica-core p(NIPAM-co-DAAM)-shell pNIPAM-shell (*left*) and a corresponding hollow microgel (*right*).

[1] J. Dubbert, K. Nothdurft, M. Karg, W. Richtering, Macromolecular Rapid Communications **36**, 159 (2015)
[2] M. Brugnoni, A. Scotti, A.A. Rudov, A.P.H. Gelissen, T. Caumanns, A. Radulescu, T. Eckert, A. Pich, I.I. Potemkin, W. Richtering, Macromolecules **51**, 2662 (2018)
[3] J.D. Debord, L.A. Lyon, Langmuir **19**, 7662 (2003)
[4] J. Dubbert, T. Honold, J.S. Pedersen, A. Radulescu, M. Drechsler, M. Karg, W. Richtering, Macromolecules **47**, 8700 (2014)
[5] A. Scotti, S. Bochenek, M. Brugnoni, M.A. Fernandez-Rodriguez, M.F. Schulte, J.E. Houston, A.P.H. Gelissen, I.I. Potemkin, L. Isa, W. Richtering, Nature Communications **10**, 1418 (2019)
[6] A. Scotti, A.R. Denton, M. Brugnoni, J.E. Houston, R. Schweins, I.I. Potemkin, W. Richtering, Macromolecules **52**, 3995 (2019)
[7] A. Scotti, M. Brugnoni, C.G. Lopez, S. Bochenek, J.J. Crassous, W. Richtering, Soft Matter **16**, 668 (2020)
[8] M. Stieger, W. Richtering, J.S. Pedersen, P. Lindner, The Journal of Chemical Physics **120**, 6197 (2004)